Imaging of integrin $\alpha_v\beta_3$ expression in patients with malignant glioma by [^{18}F] Galacto-RGD positron emission tomography

Oliver Schnell, Bjarne Krebs, Janette Carlsen, Isabelle Miederer, Claudia Goetz, Roland H. Goldbrunner, Hans-Jürgen Wester, Roland Haubner, Gabriele Pöpperl, Markus Holtmannspötter, Hans A. Kretzschmar, Horst Kessler, Jörg-Christian Tonn, Markus Schwaiger, and Ambros J. Beer

Department of Neurosurgery (O.S., C.G., R.H.G., J.-C.T.), Center for Neuropathology and Prion Research (B.K., H.A.K.), Department of Nuclear Medicine (G.P.), and Department of Neuroradiology (M.H.), Klinikum Grosshadern, Ludwig-Maximilians-Universität München, Munich, Germany; Department of Nuclear Medicine, Klinikum rechts der Isar, Technische Universität München, Munich, Germany (J.C., I.M., H.-J.W., M.S., A.J.B.); Universitätsklinik für Nuklearmedizin, Medizinische Universität Innsbruck, Austria (R.H.); Center of Integrated Protein Science, Department of Chemistry, Technische Universität München, Garching, Germany (H.K.)

Inhibitors targeting the integrin $\alpha_v\beta_3$ are promising new agents currently tested in clinical trials for supplemental therapy of glioblastoma multiforme (GBM). The aim of our study was to evaluate ^{18}F-labeled glycosylated Arg-Gly-Asp peptide ([^{18}F]Galacto-RGD) PET for noninvasive imaging of $\alpha_v\beta_3$ expression in patients with GBM, suggesting eligibility for this kind of additional treatment. Patients with suspected or recurrent GBM were examined with [^{18}F]Galacto-RGD PET. Standardized uptake values (SUVs) of tumor hotspots, galea, and blood pool were derived by region-of-interest analysis. [^{18}F]Galacto-RGD PET images were fused with cranial MR images for image-guided surgery. Tumor samples taken from areas with intense tracer accumulation in the [^{18}F]Galacto-RGD PET images and were analyzed histologically and immunohistochemically for $\alpha_v\beta_3$ integrin expression. While normal brain tissue did not show significant tracer accumulation (mean SUV, 0.09 ± 0.04), GBMs demonstrated significant but heterogeneous tracer uptake, with a maximum in the highly proliferating and infiltrating areas of tumors (mean SUV, 1.6 ± 0.5). Immunohistochemical staining was prominent in tumor microvessels as well as glial tumor cells. In areas of highly proliferating glial tumor cells, tracer uptake (SUVs) in the [^{18}F]Galacto-RGD PET images correlated with immunohistochemical $\alpha_v\beta_3$ integrin expression of corresponding tumor samples. These data suggest that [^{18}F] Galacto-RGD PET successfully identifies $\alpha_v\beta_3$ expression in patients with GBM and might be a promising tool for planning and monitoring individualized cancer therapies targeting this integrin. *Neuro-Oncology 11, 861–870, 2009 (Posted to Neuro-Oncology [serial online], Doc. D08-00188, April 28, 2009. URL http://neuro-oncology.dukejournals.org; DOI: 10.1215/15228517-2009-024)*

Keywords: $\alpha_v\beta_3$, [^{18}F]Galacto-RGD, malignant glioma, PET, integrins

Received July 17, 2008; accepted February 25, 2009.

Address correspondence to Ambros J. Beer, Department of Nuclear Medicine, Klinikum rechts der Isar, Technische Universität München, Ismaninger Strasse 22, 81675 Munich, Germany (beer@roe.med.tum.de).

Glioblastoma multiforme (GBM) is the most common and also the most aggressive brain tumor type, which comprises different histological variants and molecular pathologies.[1–3] There is growing

evidence that therapeutic options for patients with GBM have to consider such molecular signatures as O^6-methylguanine methyltransferase promoter methylation status or chromosomal aberrations (e.g., loss of heterozygosity on chromosomes 1p and 19q) of each individual patient to meet the need for a more personalized medicine in the modern treatment concepts for cancer patients.[4–6] Integrin $\alpha_v\beta_3$ has been studied thoroughly as a potential target for antiangiogenic therapy in cancer and led to the development of multiple $\alpha_v\beta_3$ inhibitors, which are currently being evaluated in clinical trials.[7–9] In patients with recurrent GBM, the $\alpha_v\beta_3$ antagonist EMD121974 developed in our laboratory[10] (cilengitide; Merck KG, Darmstadt, Germany) has recently shown promising results as a salvage treatment option, with good tolerance of the drug.[11] Moreover, preliminary data demonstrate a significant benefit for patients with newly diagnosed GBM receiving concomitant radiochemotherapy with temozolomide and supplemental administration of this $\alpha_v\beta_3$ antagonist.[12] However, for several tumor entities, the level of $\alpha_v\beta_3$ expression varies considerably among individual patients.[13–15] Recently, we have demonstrated that expression of $\alpha_v\beta_3$ integrin is also very heterogeneous in patients with primary GBM.[16] Therefore, it would be important to select patients with high $\alpha_v\beta_3$ integrin expression for potential treatment with $\alpha_v\beta_3$-specific antagonists. Molecular imaging by PET lends itself to these purposes, as it allows for noninvasive determination of biological tumor characteristics.[17] We have therefore developed the PET tracer ^{18}F-labeled glycosylated Arg-Gly-Asp peptide ([^{18}F]Galacto-RGD) for noninvasive assessment of $\alpha_v\beta_3$ expression.[15] In vitro and preclinical in tumor xenografts showed that [^{18}F]Galacto-RGD binds selectively and specifically to $\alpha_v\beta_3$ integrin.[18] In systemic tumors, [^{18}F]Galacto-RGD PET has been shown to be suitable for noninvasive assessment of the level of $\alpha_v\beta_3$ expression in murine tumor models as well as in patients.[19,20] In this study, we investigated for the first time the patterns of [^{18}F]Galacto-RGD uptake in the CNS in patients with GBM and compared them with expression of $\alpha_v\beta_3$ integrin by correlating tracer uptake with immunohistochemistry of corresponding tumor samples.

Materials and Methods

Radiopharmaceutical Preparation

Synthesis of the labeling precursor and subsequent ^{18}F-labeling were performed as described previously.[21] Integrity of [^{18}F]Galacto-RGD was controlled by reverse-phase high-performance liquid chromatography before injection for every synthesis. The injected activity per patient was between 105 and 192 MBq (mean, 160.3 ± 40.1 MBq).

Patients

This study was approved by the ethics committee of the Techniche Universität München, Munich, Germany, and informed written consent was obtained from all patients. Twelve patients were included in the study (Table 1). Inclusion criteria consisted of clinically and/or MRI-based suspected primary or known recurrent GBM, >18 years of age, and the ability to give written and informed consent. Exclusion criteria were pregnancy, lactation period, and impaired renal function (serum creatinine level > 1.2 mg/dl).

The tumors were analyzed postoperatively by histological investigation according to the WHO criteria.[1,2] For correlation between [^{18}F]Galacto-RGD tracer accumulation and immunohistochemical $\alpha_v\beta_3$ integrin expression, only patients with histologically confirmed de novo or recurrent GBM (WHO grade IV) were analyzed.

Table 1. Demographics, pathology/treatments, and scan protocols of study population

Patient	Age (Years)	Sex	Pathology	Treatment prior to PET	SUV Tumor	Tumor:Blood Ratio	Tumor DV_{tot}	CoV (%)
1	36	M	GBM left temporal lobe; recurrent disease	TR, EBR	0.9	0.6	#	#
2	57	F	GBM right temporal lobe; newly diagnosed	None	1.8	2.0	0.90	3.0
3	64	F	GBM right temporo-occipital lobe; recurrent disease	TR, EBR	2.8	1.9	1.38	19.7
4	63	F	GBM left frontal lobe; newly diagnosed	None	0.8	0.8	0.46	11.2
5	70	F	GBM left parieto-occipital lobe; recurrent disease	TR	N.A.	N.A.	#	#
6	42	M	Metastasis from adenocarcinoma (of the lung) right parietal lobe; newly diagnosed	None	1.3	1.2	#	#
7	61	F	GBM left frontal lobe; newly diagnosed	None	1.8	1.8	#	#
8	69	M	GBM left occipital lobe; recurrent disease	TR, EBR, RIT	2.0	2.0	#	#
9	78	M	GBM right parietal lobe; newly diagnosed	None	2.1	1.6	1.67	15.4
10	39	M	GBM multifocal; recurrent disease	TR	1.2	1.2	1.2	8.6
					1.6	1.6	2.0	107.1
11	30	F	GBM right frontal lobe; recurrent disease	TR	1.3	1.6	0.87	9.9
12	66	F	GBM right parietal lobe; recurrent disease	TR	1.8	1.7	0.9	20.6

Abbreviations: SUV, standardized uptake value; DV_{tot}, total distribution volume; CoV, coefficient of variation; GBM, glioblastoma multiforme; TR, gross total tumor resection; EBR, external beam radiation (60 Gy); N.A., no tracer accumulation in residual tumor visible; RIT, local radioimmunotherapy; #, only static emission scans.

PET Procedure

Imaging was performed with either an ECAT EXACT HR$^+$ (n = 2) or an ECAT EXACT (n = 10) PET scanner (CTI/Siemens, Knoxville, TN, USA) as described previously for other solid tumors.[20] In seven patients, within 60 min after bolus injection of the tracer, dynamic emission scans of 22 frames were acquired covering the region of the tumor in order to obtain time–activity curves (TACs), as described previously.[15] In the remaining five patients, one static emission scan from 40 to 60 min after injection was acquired covering the tumor region.

Image Analysis of Biodistribution Data

Positron emission data were reconstructed using the ordered-subsets expectation maximization algorithm (eight iterations, four subsets). For image analysis, CAPP software version 7.1 (CTI/Siemens) was used. Attenuation-corrected images were calibrated to standardized uptake values (SUVs) or to Bq/ml.[22] In the static emission scans 40–60 min postinjection (p.i.) or in the summarized images from 40 to 60 min p.i. from the dynamic scans, circular regions of interest (ROIs) were placed over the tumor area with the maximum activity, the galea, the normal brain contralateral to the lesions, and the superior sagittal sinus by an experienced operator (A.J.B.). The diameter of the ROIs was set to 0.8 cm.

Kinetic Modeling

The selection of TACs and subsequent kinetic analyses were performed using the PMOD medical imaging program, version 2.5 (PMOD Group, Zurich, Switzerland). An ROI approach was applied to the dynamic images in order to obtain TACs for lesions as well as for background tissue (galea). In the case of tumor tissue, polygonal ROIs were drawn over the whole tumor in all slices with visible tumor uptake. Circular ROIs with a diameter of 0.8 mm were drawn over the galea in the whole volume of interest, and image analysis was performed as described previously.[15,23] Various compartment models were fitted to the data, and kinetic constants were estimated by minimizing the sum of squared differences between the tissue TACs and the model-predicted curves. The total distribution volume (DV_{tot}) was calculated for all ROIs based on the directly estimated kinetic rate constants (K_1–k_4). A more detailed description of the compartment models and the mathematical definition of DV_{tot} can be found elsewhere.[24–26]

Magnetic Resonance Imaging

MRI was performed on a 1.5-T scanner (Magnetom Vision, Siemens, Erlangen, Germany) using a standard bird-cage head coil. A contrast-enhanced (intravenous administration of gadolinium-diethylenetriamine penta acetate (DTPA) at a concentration of 0.2 mmol/kg body weight [Magnevist; Schering, Berlin, Germany]) T_1-weighted three-dimensional volume was acquired routinely in each patient with a magnetization-prepared rapid-gradient echo sequence (repetition time = 11.4 ms; echo time = 4.4 ms; flip angle = 15°, with a 256 mm × 205 mm field of view and a voxel size of 1 mm × 1 mm × 1.5 mm). Continuous 2-mm axial slices with no interslice gap were reconstructed from the acquired data sets and were used for image fusion, as described below.

Surgical Procedure

Five patients with either suspected (n = 2) or recurrent (n = 3) GBM received tumor resection using image-guided surgery. PET images and MRI scans were matched (iPlan-software; BrainLAB AG, Feldkirchen, Germany) to define biopsy areas on the cranial MR images with high as well as low SUVs in the [^{18}F]Galacto-RGD PET images. After induction of general anesthesia, the head was fixed in a three-point head clamp (Mayfield; Integra LifeSciences Corp., Cincinnati, OH, USA) secured to the operation table. After attaching a reference star to the table, patient registration was performed with a Z-Touch wireless laser (BrainLAB AG) utilizing the surface anatomy of the patient's face and head to calculate an advanced surface-matching algorithm. Intraoperative image guidance was achieved with a mobile navigation platform (VectorVision 2, BrainLAB AG), which allowed a three-dimensional orientation of the biopsy target point in coronal, axial, and sagittal MRI planes. After standard craniotomy procedures, the tumor region was uncovered and frameless tumor biopsy samples (n = 21) were taken from the preoperatively defined areas according to intraoperative MRI guidance.

Immunohistochemistry

Immunohistochemical staining procedures were performed as described previously.[16] In brief, tumor samples were snap frozen, sectioned (6 μm), and mounted on glass slides (SuperFrost plus, Menzel, Braunschweig, Germany). After fixation (4% buffered formaldehyde and acetone, 10 min at 4°C each), a short equilibration (phosphate-buffered saline, pH 7.3) was added. The specimens were then stained simultaneously by an automated slide-stain robot (BenchMark and NexES software, version 9.20; Ventana, Strasbourg, France), including an endogenous biotin-blocking step and antigen retrieval. The primary monoclonal anti-$\alpha_v\beta_3$ integrin antibody (1:100; clone LM609, Chemicon, Temecula, CA, USA) or monoclonal anti-CD31 (1:50; DakoCytomation, Hamburg, Germany) and polyclonal biotinylated secondary antibodies (1:150, DakoCytomation) were incubated over 32 min at 37°C. The detection was gained by conjugated streptavidin horseradish peroxidase (prediluted/ready to use; Ventana) and visualized by generation of 3,3'-diaminobenzidine tetrahydrochloride (DAB) chromogen with hydrogen peroxide substrate. The counterstain followed, with hematoxylin.

Analysis of Immunohistochemical Staining

For maximum accuracy, $\alpha_v\beta_3$-integrin was immunohistochemically detected by imaging software, which was calibrated for this purpose, as described elsewhere with slight modifications.[16] All sections were scanned by constant light and magnification setting (983 μm × 737 μm). Then a "zero point" was set to unstained tissue. The maximum staining intensity of 100% was defined by the characteristics of an $\alpha_v\beta_3$-integrin–overexpressing human melanoma cell line (M21).[19,27] Within a selected area in the desired section, the software measured the relative mean staining intensity of the DAB (brown). The fraction of tissue detected as positive at a desired immunohistochemical staining intensity (~30% and 60% of positive control) was then determined (software written by B.K.; for details, see Vonlaufen et al.[13]). In contrast to the subjective operator's visual evaluation, the computed intensity measurements and their calibration to parallel stained positive controls provide precise values and highly reproducible results that minimized bias effects and variation in immunohistochemical staining procedures.

Statistical Analysis

All quantitative data are expressed as mean ± standard deviation. The correlation between quantitative parameters was evaluated by linear regression analysis. All statistical tests were performed at the 5% level of statistical significance, using SPSS, version 16.0 (SPSS, Inc., Chicago, IL, USA).

Results

Patient Characteristics

Inclusion criteria were fulfilled by 12 patients (eight women, four men) with a mean age of 55.3 ± 16.4 years (range, 36–78 years). Five patients presented with a short history of clinical symptoms or newly diagnosed neurological deficits suggesting GBM (WHO grade IV). The other patients (n = 7) had already been diagnosed with GBM (WHO grade IV) and had undergone different treatment modalities prior to tumor recurrence (Table 1).

Magnetic Resonance Imaging

MRI scans demonstrated typical lesions with peripheral inhomogeneous, irregular contrast enhancement and hypointense center on T_1 with gadolinium-DTPA and adjacent vasogenic edema on T_2-weighted images. There were no obvious differences in the radiological findings between suspected or recurrent GBM patients. The [^{18}F]Galacto-RGD PET scans provided corresponding molecular images with regions of tracer accumulation. Fusion of T_1 + gadolinium-DTPA MR images with [^{18}F]Galacto-RGD PET images revealed high focal activity with tracer accumulation in the tumor region (Fig. 1), which qualitatively corresponded to the areas of gadolinium-DTPA contrast enhancement, whereas the hypointense center of the tumors generally showed no tracer accumulation.

Static-Emission [^{18}F]Galacto-RGD PET Scans

In normal brain tissue, no significant tracer accumulation was visible (mean SUV, 0.09 ± 0.04). In the galea, mean tracer uptake was also uniformly low (mean SUV, 1.0 ± 0.1), but higher compared with normal brain tissue. In 11 of 12 patients, tumor tracer uptake was detectable with weak to moderate tracer accumulation within the tumor lesion (Fig. 1). Tracer uptake was heterogeneous in appearance and restricted to the periphery of the tumor, with no activity in the necrotic center of the lesions (SUV range, 0.8–2.8; mean, 1.6 ± 0.5). The mean tumor:blood, tumor:galea, and tumor:brain ratios were 1.5 ± 0.5, 1.6 ± 0.5, and 24.0 ± 26.1, respectively (Table 1).

Dynamic Emission [^{18}F]Galacto-RGD PET Scans

The kinetic modeling analysis of [^{18}F]Galacto-RGD in malignant gliomas showed a good fit of a two-tissue compartmental model with good parameter precision for tumor tissue (mean DV_{tot}, 1.18 ± 0.46; coefficient of

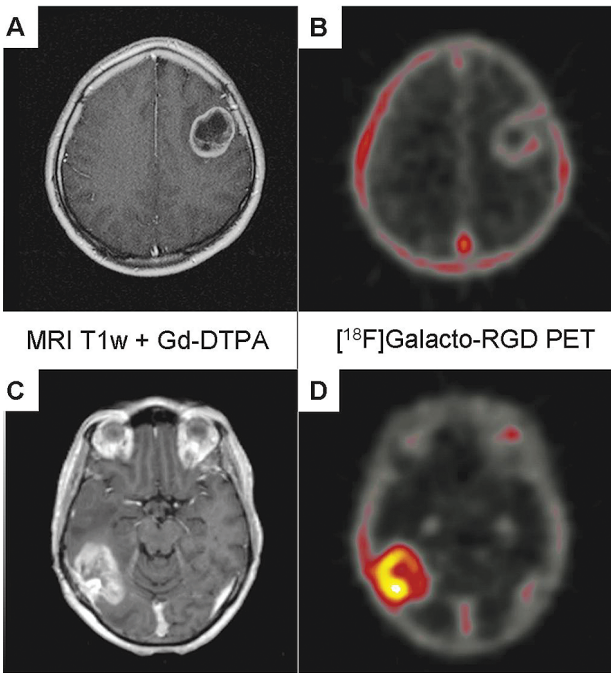

Fig. 1. Examples of patients with glioblastoma multiforme of the left frontal lobe (A, B) and right parieto-occipital lobe (C, D). Note the intense peripheral enhancement in the gadolinium-DTPA–enhanced MRI scans in both tumors (A, C). However, the tumor in B shows only very faint tracer uptake in the [^{18}F]Galacto-RGD PET (maximum standardized uptake value [SUV_{max}], 1.2), whereas the tumor in D demonstrates substantially more intense [^{18}F]Galacto-RGD uptake (SUV_{max}, 2.8).

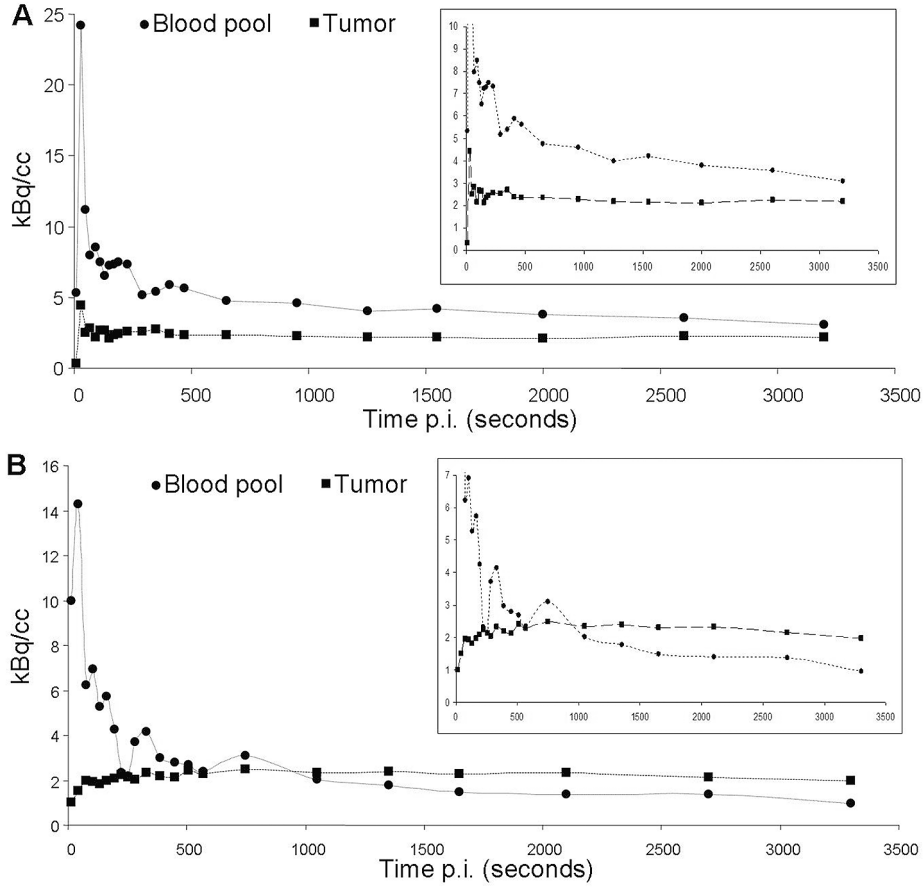

Fig. 2. Examples of time–activity curves of patients with the lowest tumor uptake (A; maximum standardized uptake value [SUV_{max}], 0.8) and the highest tumor uptake (B; SUV_{max}, 2.8). Insets show the same curves with the y-axis expanded. Note the rapid tracer washout from blood pool in both scans. (A) Low tracer accumulation in the tumor that is always below the blood pool activity and follows the tracer concentration in the blood pool, with a rapid first peak followed by a slight decrease of tracer uptake. (B) Slow tracer accumulation over the first approximately 20 min, followed by a plateau phase that is above the level of blood pool activity, indicating specific tracer binding.

variation [CoV], 24.44% ± 31.72%). The dynamic scans showed rapid tracer washout from the blood pool and rising tracer concentration in the tumors over approximately 30 min p.i., followed by a plateau phase with no substantial changes of tracer uptake until the end of the measurement at 60 min p.i. Thus, the time point for analysis of SUVs in images acquired from 40 to 60 min p.i. seems appropriate as the tracer uptake was relatively stable during this time frame. Although later measurements might have improved tumor:blood ratios slightly due to decreasing tracer concentration in the blood pool, the tracer uptake in the tumors does not seem to rise substantially after 60 min p.i. Furthermore, due to the rather rapid decay of [^{18}F], signal intensity becomes lower at later imaging time points, which again deteriorates image quality. In background tissue (galea), a one-tissue compartment model fitted best and resulted in low DV_{tot} values (mean DV_{tot}, 0.40 ± 0.11; CoV, 3.72% ± 0.60%; Fig. 2). The primary goal of the kinetic modeling study was to evaluate the quality of the tracer dynamics in GBM. However, we did not intend to exactly quantify receptor expression. For this purpose, a more invasive approach, including arterial blood sampling to generate exact arterial input functions, would have been necessary.

Histological Analysis

The diagnosis of GBM (WHO grade IV) was confirmed by routine neuropathological examination for histological grading from the overall tumor resection material of five patients. One patient with suspected GBM on MRI was excluded from further analysis because histology of the tumor samples revealed a metastasis from an adenocarcinoma. The different GBM samples (n = 21) from the remaining patients (n = 4) included areas with dense tumor growth and extensive proliferation of pleomorphic glial cells (central part of infiltrating zone = zone A; n = 10) as well as tumor cells surrounding normal brain tissue (outer rim of infiltrating zone = zone C; n = 6) or other samples with tumor adjacent to necrotic areas (inner rim of infiltrating zone = zone B; n = 5).

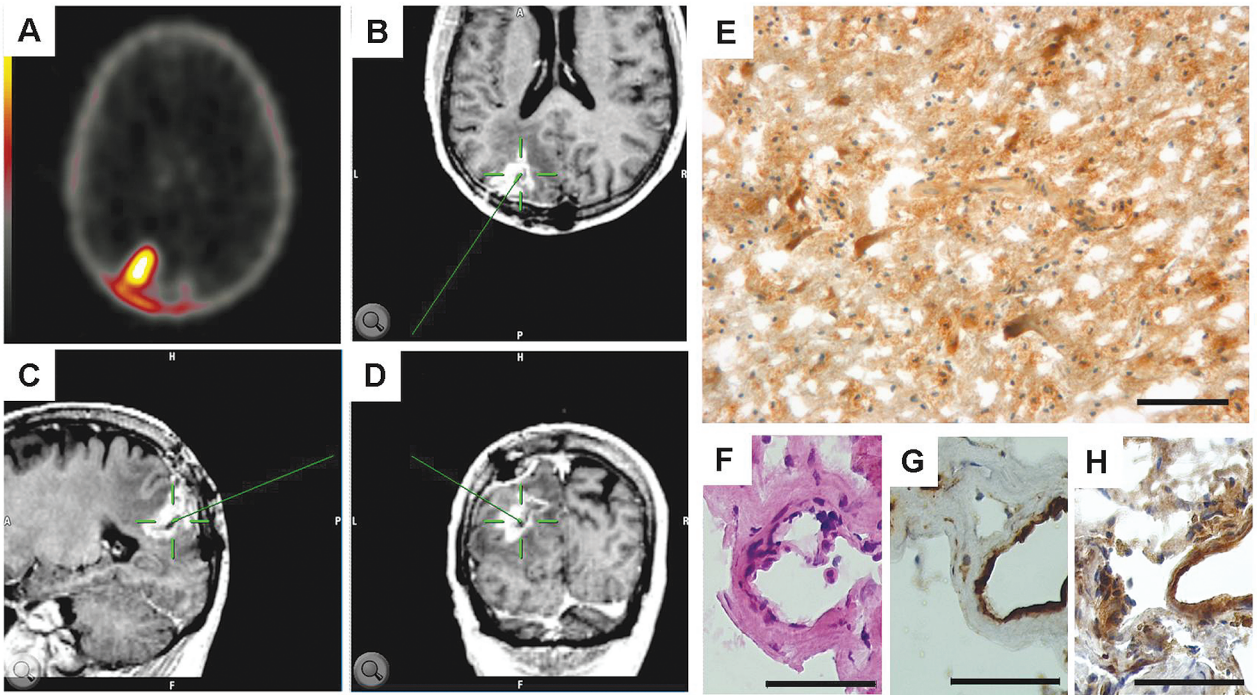

Fig. 3. Screen shot of the BrainLAB software used for image-guided surgery in a patient with a large glioblastoma multiforme of the left occipital lobe. (A) One of several preoperatively acquired corresponding [^{18}F]Galacto-RGD PET images (maximum standardized uptake value, 2.0) used for determination of the region of interest for tumor probe collection. (B–D) The neuronavigation system displays the area where tumor probes were taken before tumor resection in all three planes (axial, B; sagittal, C; coronal, D). The pointer tool targets the selected area (green). (E) Immunohistochemistry demonstrates intense $\alpha_v\beta_3$ expression in the tissue sample. (F–H) Higher magnification of serial sections from this tumor stained with hematoxylin and eosin (F), the endothelial cell marker CD31 (G), and $\alpha_v\beta_3$ integrin (H) demonstrates that the integrin expression is not restricted to the tumor vasculature but is also present in the glial tumor cells. Scale bars: E, 100 μm; F–H, 50 μm.

Immunohistochemistry of $\alpha_v\beta_3$ Expression

For immunohistochemical analysis, tumor samples (n = 21) from four patients were taken via image-guided surgery from the preoperatively defined areas of tracer accumulation in the [^{18}F]Galacto-RGD PET (Fig. 3). Immunohistochemical staining for $\alpha_v\beta_3$ confirmed a very heterogeneous integrin expression in the present samples. The different tumor parts, zones A–C, showed an inhomogeneous expression pattern depending on the character of glial tumor cells and microvascular structures. A strong immunoreactivity for the $\alpha_v\beta_3$ integrin was obvious in areas of dense tumor growth as well in numerous enlarged giant pleomorphic tumor cells. The expression of $\alpha_v\beta_3$ integrin found in microvessels was detectable mainly in the luminal (endothelial) layer, with considerably lower expression in the outer layer and surrounding perivascular area. Whereas normal brain tissue was negative for $\alpha_v\beta_3$ integrin expression, the necrotic areas in the center of the tumors showed diffuse integrin $\alpha_v\beta_3$ staining without cellular correlation. Therefore, tumor samples from these areas were deliberately excluded from correlation analysis of staining intensity and SUVs in the [^{18}F]Galacto-RGD PET images.

Semiquantitative Analysis of $\alpha_v\beta_3$ Expression via Imaging Software

Immunohistochemical detection of $\alpha_v\beta_3$ integrin was calibrated to xenotransplanted $\alpha_v\beta_3$-positive human melanoma cells (M21; expression set to 100%). The overall mean staining intensity of $\alpha_v\beta_3$ integrin in the samples analyzed reached 75.06% ± 14.65%. The fraction of immunohistochemically positive structures, which was calculated for moderate (~30% of positive control) and strong (~60% of positive control) $\alpha_v\beta_3$ integrin expression levels, was 20.45% ± 19.8% and 3.15% ± 4.35%, respectively. To investigate the expression pattern in more detail, integrin expression was analyzed in different parts of the active tumor and calculated separately for zone A (n = 5), zone B (n = 10), and zone C (n = 6). This subanalysis confirmed that the integrin expression is most prominent in the most active part of the vital tumor (zone B; see Table 2).

These findings were in accordance with [^{18}F]Galacto-RGD PET images, where the maximum tracer uptake (SUV) was present in the highly proliferating and infiltrating areas of the tumors (zone B, 1.81; zone C, 1.42; zone A, 1.23). The various tumor parts and their expression patterns are demonstrated in Fig. 4 and Table 2.

Table 2. Statistical analysis of $\alpha_v\beta_3$ integrin immunohistochemistry from different parts of the vital tumor area

Infiltrating Zone	Mean Staining Intensity	Moderately Stained Area	Strongly Stained Area
Zone A	77.19% ± 15.01	26.6% ± 20.51%	3.86% ± 4.76%
Zone B	68.28% ± 11.99	16.65% ± 18.79%	2.0% ± 2.85%
Zone C	78.93% ± 14.1	12.71% ± 15.12%	3.11% ± 4.68%

Integrin expression was detected by calculating the mean staining intensity and moderately and strongly stained tumor fractions from different areas of the infiltrating zone: the central part (zone A), the inner rim (next to necrosis; zone B), and the outer rim (next to normal brain tissue; zone C).

Correlation of [^{18}F]Galacto-RGD Tracer Accumulation and Immunohistochemical $\alpha_v\beta_3$ Integrin Expression

In order to compare the results of tracer accumulation (SUVs) from [^{18}F]Galacto-RGD PET images with the immunohistochemical $\alpha_v\beta_3$ integrin expression in patients with malignant gliomas, corresponding samples of both analysis were matched. Analyzing all tissue samples resulted in a weak but significant correlation between tracer uptake and immunohistochemical staining intensity of $\alpha_v\beta_3$ expression ($r = 0.463$, $p = 0.034$). Since $\alpha_v\beta_3$ integrin expression is very heterogeneous in malignant gliomas and due to the rather small size of the immunohistochemically analyzed probes (average size, 2 mm^3), staining intensities varied among probes from adjacent areas, as described above. Therefore, each sample displayed only a fraction from the larger-size PET voxel analyzed for detection of [^{18}F]Galacto-RGD uptake, represented via detection of SUVs. Despite all this, a subanalysis from the central part of the vital tumor (zone B; $n = 10$ tumor samples from four different patients) comparing SUVs and $\alpha_v\beta_3$ integrin staining intensity also showed a moderate but significant correlation ($r = 0.602$, $p = 0.032$; Fig. 5A). These results provide further evidence that the noninvasive detection of $\alpha_v\beta_3$ integrin expression in patients with malignant gliomas with [^{18}F]Galacto-RGD PET is feasible and seems to be a promising tool to monitor clinical therapies targeting this integrin.

Microvessel-Associated Expression of $\alpha_v\beta_3$ Integrin

Because [^{18}F]Galacto-RGD and therapeutic regimens may target primarily $\alpha_v\beta_3$ integrin expressed in small proliferating tumor vessels, we additionally performed a subanalysis to investigate the impact of the micro-

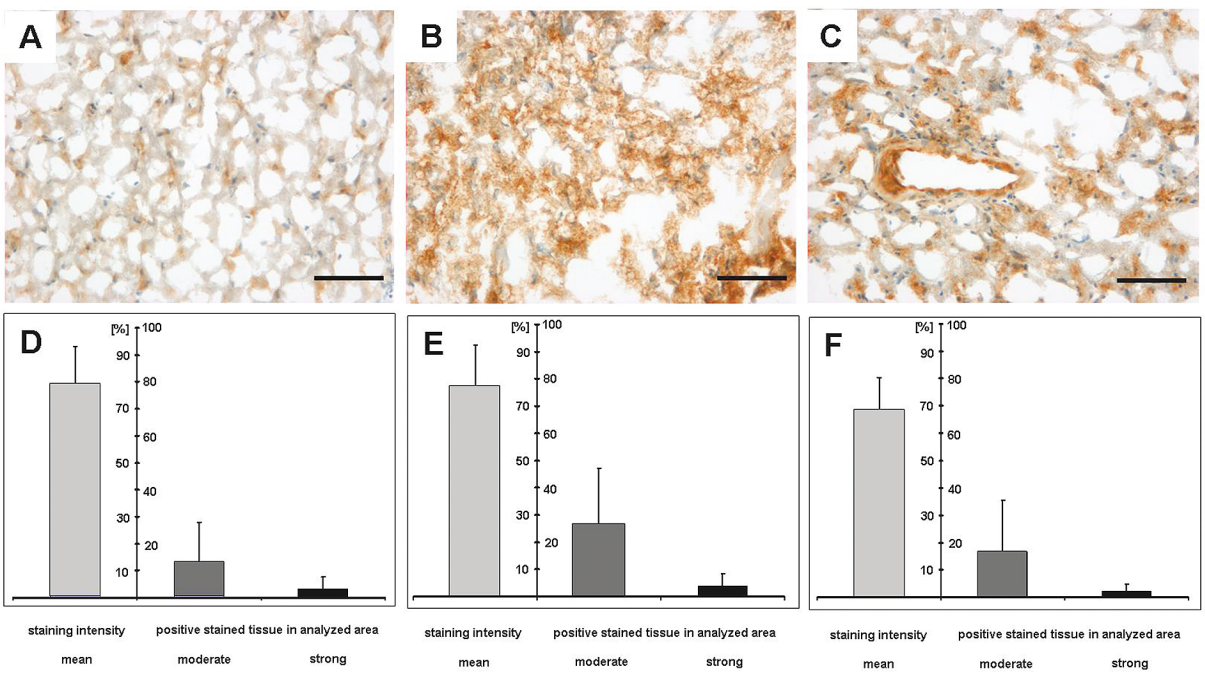

Fig. 4. Immunohistochemistry (A–C) and statistical analysis of $\alpha_v\beta_3$ expression (D–F) within the different parts of the active tumor: center of the tumor (next to the tumor necrosis = zone A; A and D), the central part of the vital tumor (zone B; B and E), and the infiltrating zone (next to the normal brain tissue = zone C; C and F). (D–F) Mean staining intensities (indicated as percentage of positive control [M21 set to 100%]) as well as the fraction of moderately or strongly stained $\alpha_v\beta_3$-positive tissue within the tumor probes (percentage of the analyzed area). This subanalysis confirmed that the integrin expression is most prominent in the most active (central) part of the vital tumor (zone B; B and E). Scale bars, 100 μm for A–C.

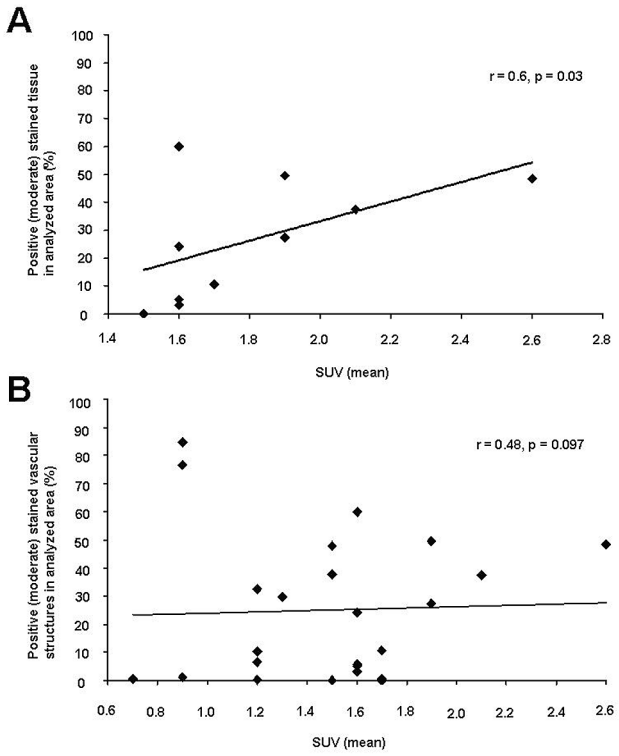

Fig. 5. Correlation subanalysis of staining intensity of $\alpha_v\beta_3$ expression and corresponding standardized uptake values (SUVs) measured according to the biopsy sites determined by image-guided surgery. (A) There is a moderate but significant correlation between staining intensity of $\alpha_v\beta_3$ expression and tracer uptake in the central part of the vital tumor (zone B; $r = 0.602$, $p = 0.032$). (B) There was only a tendency but no significant correlation for small-vessel–associated $\alpha_v\beta_3$ integrin expression with the corresponding SUVs ($r = 0.476$, $p = 0.097$), suggesting that the integrin expression detected via [^{18}F]Galacto-RGD PET is not solely vessel associated.

vessel-dependent $\alpha_v\beta_3$ integrin expression in GBM. For this examination, only proliferating vessels surrounded by vital tumor cells were measured, which resulted in a low number of samples (19 vessels in nine samples correlated with eight corresponding SUV). The small-vessel–associated expression of $\alpha_v\beta_3$ integrin was in the same range as the overall tumor tissue (mean intensity, 74.4% ± 18.1%). In comparison with the tracer uptake in [^{18}F]Galacto-RGD PET images, we found a tendency but no significant correlation of integrin expression with the corresponding SUVs ($r = 0.476$, $p = 0.097$; Fig. 5B). Taken together with the results from the overall tissue analysis, these findings suggest that the integrin expression detected noninvasively via [^{18}F]Galacto-RGD PET is not solely vessel associated.

Discussion

Targeted therapies are an important part of modern cancer treatment concepts. Ideally, they are supported by noninvasive imaging methods to detect the tumor target. In malignant gliomas, $\alpha_v\beta_3$ integrin has been appointed a key player for tumor invasion and angiogenesis. In this study, we have shown for the first time that noninvasive imaging of $\alpha_v\beta_3$ expression is feasible in patients with GBMs using [^{18}F]Galacto-RGD and PET. Although tracer uptake was weak to moderate in the tumors, it correlated significantly with the immunohistochemically determined intensity of $\alpha_v\beta_3$ expression.

Although [^{18}F]Galacto-RGD PET has been extensively studied in systemic tumors, CNS lesions such as malignant gliomas have not been studied systematically for noninvasive imaging of $\alpha_v\beta_3$ integrin expression in humans with molecular imaging techniques.[18–20] In our study, tumors were detected by [^{18}F]Galacto-RGD PET with good tumor-to-background contrast. Notably, comparing SUVs in different tumor areas with the staining intensity of $\alpha_v\beta_3$-specific immunohistochemistry in tissue samples from these areas demonstrated a significant correlation between these two parameters. Therefore, the feasibility of noninvasive imaging of $\alpha_v\beta_3$ expression in patients with GBMs using [^{18}F]Galacto-RGD and PET is supported by the present study. Moreover, the kinetic modeling analysis showed a good fit of a two-tissue compartmental model with good parameter precision for tumor tissue. The dynamic data in CNS tumors qualitatively corresponded well with the data we have acquired in systemic tumors, where we have already demonstrated selective and specific binding of [^{18}F]Galacto-RGD to $\alpha_v\beta_3$ integrin.[15,23] These data therefore suggest specific tracer binding of [^{18}F]Galacto-RGD in malignant gliomas. However, a kinetic modeling analysis can never prove but only suggest specific tracer binding, because nonspecific tracer leakage might contribute substantially to the results. Other limitations also have to be taken into account when interpreting our results.

First, the tracer uptake in GBM was substantially lower than in $\alpha_v\beta_3$-expressing tumors of the body in our previous studies.[20,22,28] Comparative measurements of the intensity of $\alpha_v\beta_3$ expression in gliomas and non-CNS tumors by immunohistochemistry and Western blotting of our group suggested only slightly lower $\alpha_v\beta_3$ expression in malignant gliomas.[16] This might in part be due to partial volume effects, which might falsely diminish the results of SUV measurements in GBM. Previous measurements with phantoms on our PET scanner have demonstrated that in lesions smaller than a diameter of approximately 2.5 cm, partial volume effects have to be taken into account, especially in regions with high tumor-to-background contrast, which applies to our study.[29] Although the total tumor diameter was usually larger than 2.5 cm, the areas of tracer uptake and of SUV measurements were mostly in the periphery of the tumors and thus usually smaller than 2.5 cm in diameter. Therefore, this technique has limitations in small tumors, and the influence of partial volume effects might in part explain why the SUVs were lower compared with our previously published results in non-CNS tumors, which mostly were larger than 2.5 cm in diameter.[15,30]

Second, factors specific for CNS tumors, such as influences of the blood-brain barrier, have to be taken into account as well. The uptake of [^{18}F]Galacto-RGD

in normal brain was even lower than that in the galea, although in both tissues no substantial $\alpha_v\beta_3$ expression and thus no tracer uptake is expected.[8] This difference in tracer retention suggests that [^{18}F]Galacto-RGD does not cross the intact blood-brain barrier. Although the accumulation of gadolinium-DTPA in the MRI scans demonstrated at least partial disruption of the blood-brain barrier in all tumors, restricted access of [^{18}F] Galacto-RGD to some tumor areas cannot be excluded. Yet, our results demonstrating that tracer uptake in the [^{18}F]Galacto-RGD PET correlates most of all with $\alpha_v\beta_3$ integrin expression of the glial tumor cells in the vital tumor areas argue against this possibility. In fact, we have demonstrated recently that the tumor cells themselves contribute substantially to the high expression of this integrin in malignant gliomas and that expression of integrin $\alpha_v\beta_3$ is not restricted to the proliferating endothelial cells.[16] Moreover, the lack of significant correlation between microvessel-associated $\alpha_v\beta_3$ integrin expression and corresponding SUVs provides further evidence that [^{18}F]Galacto-RGD not only detects $\alpha_v\beta_3$ expression on endothelial cells but also that of the surrounding vital tumor tissue. On the other hand, nonspecific tracer leakage due to a disrupted blood-brain barrier might also contribute to the total tracer uptake. However, the significant correlation of tracer uptake and immunohistochemistry of $\alpha_v\beta_3$ expression suggests specific tracer binding, although confounding effects of nonspecific tracer leakage might in part explain the only moderate correlation. This, however, is only a hypothesis, which has to be proven in future studies, for example, by comparing [^{18}F]Galacto-RGD to nonspecific perfusion tracers, which do not cross the intact blood-brain barrier, or to data from dynamic contrast-enhanced MRI.

Third, intraoperative sampling of tumor tissue is complicated due to technical limitations. Though all samples were obtained using image-guided surgery to ensure optimum concordance with the preoperatively marked areas of high and low SUVs in [^{18}F]Galacto-RGD PET, sampling errors due to "brain shift" after craniotomy cannot be excluded at all.[31] Therefore, the correlation between $\alpha_v\beta_3$ expression and SUVs might in part be altered due to sampling errors, which are hard to exclude because the staining intensity is determined in a microscopic tumor area, whereas the SUV is determined on a macroscopic scale in a volume of several cubic millimeters. Still, this limitation is inherent to comparative studies of PET and immunohistochemistry and is hard to eliminate in clinical studies. This disadvantage might possibly be overcome by performance of frame-based stereotactic tumor biopsies, which should be evaluated in future studies.

Despite the limitations mentioned above, [^{18}F] Galacto-RGD still is the currently most extensively evaluated PET tracer for detection of $\alpha_v\beta_3$ integrin expression in clinical use for systemic tumors, and our results now demonstrate the feasibility of $\alpha_v\beta_3$ imaging with this tracer in malignant gliomas. However, our results also suggest that a direct comparison of data obtained with [^{18}F]Galacto-RGD PET in systemic tumors and CNS tumors should not be done uncritically due to potential CNS-specific factors, such as influences of the blood-brain barrier on tracer uptake.

Potential applications of [^{18}F]Galacto-RGD PET might be the selection and monitoring of patients before and during $\alpha_v\beta_3$-targeted therapies, such as with EMD121974 (cilengitide). A further potential application might be demonstrating receptor occupancy of $\alpha_v\beta_3$ antagonists by [^{18}F]Galacto-RGD PET in order to evaluate the most efficient dose in each individual patient. This might be one step implementing the concept of "individualized medicine" in clinical routine.

Acknowledgments

We thank Angelika Henn for excellent technical work on tissue preparation and immunohistochemistry, and Tim Wesemann for technical assistance concerning MR imaging and data transfer for neuronavigational purposes. This study was supported by grants from the Förderprogramm für Forschung und Lehre of the Faculty of Medicine of the Ludwig-Maximilians-Universität München (O.S.; FöFoLe, Reg.-No. 377) and from the Deutsche Forschungsgemeinschaft (C.G.; DFG-Forschergruppe Radionuklidtherapie, FOR-411).

References

1. Kleihues P, Cavenee WK. *Pathology and Genetics of Tumours of the Nervous System*. Lyon, France: IARC Press, 2000.
2. Kleihues P, Louis DN, Scheithauer BW, et al. The WHO classification of tumors of the nervous system. *J Neuropathol Exp Neurol*. 2002;61:215–225.
3. Ohgaki H, Dessen P, Jourde B, et al. Genetic pathways to glioblastoma: a population-based study. *Cancer Res*. 2004;64:6892–6899.
4. Grasbon-Frodl EM, Kreth FW, Ruiter M, et al. Intratumoral homogeneity of MGMT promoter hypermethylation as demonstrated in serial stereotactic specimens from anaplastic astrocytomas and glioblastomas. *Int J Cancer*. 2007;121:2458–2464.
5. Wen PY, Deangelis LM. Chemotherapy for low-grade gliomas: emerging consensus on its benefits. *Neurology*. 2007;68:1762–1763.
6. Stupp R, Hegi ME, Gilbert MR, et al. Chemoradiotherapy in malignant glioma: standard of care and future directions. *J Clin Oncol*. 2007;25:4127–4136.
7. Meyer A, Auernheimer J, Modlinger A, et al. Targeting RGD recognizing integrins: drug development, biomaterial research, tumor imaging and targeting. *Curr Pharm Des*. 2006;12:2723–2747.
8. Kumar CC. Integrin alpha v beta 3 as a therapeutic target for blocking tumor-induced angiogenesis. *Curr Drug Targets*. 2003;4:123–131.
9. Cai W, Chen X. Anti-angiogenic cancer therapy based on integrin alphavbeta3 antagonism. *Anticancer Agents Med Chem*. 2006;6:407–428.
10. Dechantsreiter MA, Planker E, Matha B, et al. N-Methylated cyclic RGD peptides as highly active and selective alpha(V)beta(3) integrin antagonists. *J Med Chem*. 1999;42:3033–3040.
11. Nabors LB, Mikkelsen T, Rosenfeld SS, et al. Phase I and correlative biology study of cilengitide in patients with recurrent malignant glioma. *J Clin Oncol*. 2007;25:1651–1657.
12. Reardon DA, Nabors LB, Stupp R, et al. Cilengitide: an integrin-targeting arginine-glycine-aspartic acid peptide with promising activity for glioblastoma multiforme. *Expert Opin Investig Drugs*. 2008;17:1225–1235.
13. Vonlaufen A, Wiedle G, Borisch B, et al. Integrin alpha(v)beta(3) expression in colon carcinoma correlates with survival. *Mod Pathol*. 2001;14:1126–1132.
14. Sato T, Konishi K, Kimura H, et al. Vascular integrin beta 3 and its relation to pulmonary metastasis of colorectal carcinoma. *Anticancer Res*. 2001;21:643–647.
15. Beer AJ, Haubner R, Goebel M, et al. Biodistribution and pharmacokinetics of the alphavbeta3-selective tracer 18F-Galacto-RGD in cancer patients. *J Nucl Med*. 2005;46:1333–1341.
16. Schnell O, Krebs B, Wagner E, et al. Expression of integrin alpha(v) beta(3) in gliomas correlates with tumor grade and is not restricted to tumor vasculature. *Brain Pathol*. 2008;18:378–386.
17. Weber WA. Positron emission tomography as an imaging biomarker. *J Clin Oncol*. 2006;24:3282–3292.
18. Haubner R, Wester HJ, Weber WA, et al. Noninvasive imaging of alpha(v)beta3 integrin expression using 18F-labeled RGD-containing glycopeptide and positron emission tomography. *Cancer Res*. 2001;61:1781–1785.
19. Haubner R, Weber WA, Beer AJ, et al. Noninvasive visualization of the activated alphavbeta3 integrin in cancer patients by positron emission tomography and [18F]Galacto-RGD. *PLoS Med*. 2005;2:e70.
20. Beer AJ, Haubner R, Sarbia M, et al. Positron emission tomography using [18F]Galacto-RGD identifies the level of integrin alpha(v)beta3 expression in man. *Clin Cancer Res*. 2006;12:3942–3949.
21. Haubner R, Kuhnast B, Mang C, et al. [18F]Galacto-RGD: synthesis, radiolabeling, metabolic stability, and radiation dose estimates. *Bioconjug Chem*. 2004;15:61–69.
22. Weber WA, Ziegler SI, Thodtmann R, et al. Reproducibility of metabolic measurements in malignant tumors using FDG PET. *J Nucl Med*. 1999;40:1771–1777.
23. Beer AJ, Grosu AL, Carlsen J, et al. [18F]Galacto-RGD positron emission tomography for imaging of alphavbeta3 expression on the neovasculature in patients with squamous cell carcinoma of the head and neck. *Clin Cancer Res*. 2007;13:6610–6616.
24. Carson RE. Tracer kinetic modelling in PET. In: Valk PE, Bailey DL, Townsend DW, Maisey MN, eds. *Positron Emission Tomography: Basic Science and Clinical Practice*. London: Springer-Verlag; 2003:147–180.
25. Slifstein M, Laruelle M. Models and methods for derivation of in vivo neuroreceptor parameters with PET and SPECT reversible radiotracers. *Nucl Med Biol*. 2001:28:595–608.
26. Spilker ME, Sprenger T, Valet M, et al. Quantification of [18F]diprenorphine kinetics in the human brain with compartmental and non-compartmental modeling approaches. *Neuroimage*. 2004;22:1523–1533.
27. Cheresh DA, Spiro RC. Biosynthetic and functional properties of an Arg-Gly-Asp-directed receptor involved in human melanoma cell attachment to vitronectin, fibrinogen, and von Willebrand factor. *J Biol Chem*. 1987;262:17703–17711.
28. Bello L, Francolini M, Marthyn P, et al. Alpha(v)beta3 and alpha(v) beta5 integrin expression in glioma periphery. *Neurosurgery*. 2001;49:380–389.
29. Brix G, Bellemann ME, Hauser H, et al. [Recovery coefficients for the quantification of the arterial input functions from dynamic PET measurements: experimental and theoretical determination]. *Nuklearmedizin*. 2002;41:184–190.
30. Beer AJ, Lorenzen S, Metz S, et al. Comparison of integrin alpha-Vbeta3 expression and glucose metabolism in primary and metastatic lesions in cancer patients: a PET study using 18F-Galacto-RGD and 18F-FDG. *J Nucl Med*. 2008;49:22–29.
31. Hall WA, Truwit CL. Intraoperative MR-guided neurosurgery. *J Magn Reson Imaging*. 2008;27:368–375.